

1   **Methods of incorporation of new reaction products in thermodynamic databases of**  
2   **cementitious systems**

4   Tongren Zhu,<sup>a</sup> Maria Juenger,<sup>a</sup> O. Burkan Isgor<sup>b</sup>, and Lynn E. Katz,<sup>a,\*</sup>

6   <sup>a</sup> University of Texas at Austin; Department of Civil, Architectural and Environmental Engineering; 301 E. Dean  
7   Keeton St. C1700, Austin, TX 78712, USA.

9   <sup>b</sup> Oregon State University; Civil and Construction Engineering, Corvallis, OR 97331, USA.

10   \* Corresponding author: [lynnkatz@mail.utexas.edu](mailto:lynnkatz@mail.utexas.edu)

13   **Abstract**

14   Strategic blending of supplementary cementitious materials (SCMs) into ordinary portland  
15   cement (OPC) helps reduce energy use and greenhouse gas emissions from concrete production.  
16   Expanding thermodynamic databases to include new reaction products from blended cements  
17   improves computational approaches used to understand the impact of blending SCMs with  
18   cement. Determination of thermodynamic parameters of cement reaction products based on  
19   temperature-dependent solubility is widely used in cement research; however, assumptions,  
20   limitations, and potential errors due to intercorrelation of the thermodynamic parameters in these  
21   calculation methods are rarely discussed. Here, methods for obtaining thermodynamic  
22   parameters are critically reviewed, including discussion of experimental validation. The  
23   discussion herein provides useful guidance to improve and validate the process of determining  
24   thermodynamic parameters of new reaction products from SCM-OPC reactions.

25  
26   **Keywords:** Cement reaction products; thermodynamic models; solubility

28   **1. Introduction**

29   Portland cement is the most energy intensive ingredient in concrete, the most widely used  
30   building material and second most manufactured product after potable water.[1] The production  
31   of portland cement accounts for approximately 5-8% of global carbon dioxide emissions.[2] The  
32   concrete industry has been striving toward reducing these impacts through various approaches.  
33   For example, strategic blending of supplementary cementitious materials (SCMs) into ordinary  
34   portland cement (OPC) helps reduce energy use and greenhouse gas emissions from concrete  
35   production.[3,4]. The ability to predict the reactions of cementitious materials in concrete helps  
36   optimize mixtures for different performance criteria including durability and carbon  
37   footprint.[5,6] Thermodynamic modeling allows the prediction of hydrated cement phase  
38   assemblages and chemical compositions for a variety of cementitious material combinations.[7–  
39   9] Therefore, thermodynamic modeling can provide a computational approach to facilitate  
40   understanding of the impact of blending SCMs or other materials with cement on the chemical  
41   composition of the hydrated cementitious mixture.

42   Accurate thermodynamic modeling of cementitious systems relies on accurate and complete  
43   thermodynamic databases that include all possible reactants and products of the cement  
44   reactions.[10] CEMDATA, developed by the Swiss Federal Laboratories for Materials Testing

45 and Research (EMPA), is the most widely used cement database and covers a large range of  
46 compounds that form in reactions of cementitious systems including OPC, SCMs and other  
47 binders. The latest version, CEMDATA18, is written in formats supporting both Gibbs Energy  
48 Minimization-Selector (GEMS) and PHREEQC, two thermodynamic modeling frameworks that  
49 use different approaches for modeling chemical systems.[10–12] GEMS simulates phase  
50 assemblages of the reaction products by minimizing the total Gibbs free energy of the  
51 system.[12] PHREEQC, on the other hand, is based on the law of mass action (LMA) and  
52 performs simulations by iteratively solving a system of mole balance and charge balance  
53 equations.[11] The LMA-based thermodynamic models are most commonly used in reactive  
54 transport models to calculate equilibrium speciation due to the simplicity of the  
55 algorithm.[13,14] However, since the LMA solvers have limitations when multicomponent  
56 phases (e.g., solid solutions, non-ideal liquids, and gaseous phases) are considered, the Gibbs  
57 energy minimization algorithm is generally the method of choice for simulations of complex  
58 multiphase systems.[12] As a result, cementitious systems have been traditionally modeled using  
59 GEMS, although the use of LMA-based codes, specifically PHREEQC, has been increasing for  
60 modeling cementitious systems.[15] Both GEMS and PHREEQC frameworks can be used to  
61 solve for concentrations of chemical species, their activity coefficients, chemical potentials of  
62 chemical elements, and other thermodynamic quantities such as pH, fugacities, and the redox  
63 state of the system (i.e.,  $p_e$ ). One major advantage of GEMS is its ability to calculate volume  
64 fractions of solid reaction products, as well as liquid and gas phases, so that estimates of  
65 capillary porosity and chemical shrinkage can be obtained.

66 The major limitation associated with modeling blended cement is the lack of thermodynamic  
67 data for the new solid reaction products that do not exist in the current thermodynamic databases;  
68 stoichiometry, solubility data, and thermodynamic constants required to predict temperature  
69 effects and porosity have not been determined or included in the CEMDATA database. These  
70 data need to be determined, and the compounds need to be added to the CEMDATA database to  
71 extend the application of thermodynamic modeling of reactions in cementitious systems.  
72 Because the GEMS version of the database can be converted to the PHREEQC database,[10] this  
73 paper focuses on incorporating thermodynamic data into a database for GEMS use. In a Gibbs  
74 free energy minimization model (e.g., GEMS), the overall reaction is independent of the form of  
75 the input species but depends on the stoichiometric composition of the elements in the input  
76 recipe. In GEMS, the input recipe for complex cementitious systems such as SCMs (e.g. fly ash,  
77 pumice, etc.) is usually entered in the form of total molar (or mass) concentration of each  
78 component (typically in the form of oxides) determined from chemical analysis (e.g., x-ray  
79 fluorescence (XRF)) rather than distinct chemical compounds. As long as the correct molar (or  
80 mass) inputs of elements of all the reactants are available, stoichiometry is able to describe every  
81 species in the reaction products.[12] Therefore, application of GEMS is only limited by the  
82 availability of thermodynamic parameters for new solid reaction products.[16]

83 This paper aims to provide a brief overview of the required thermodynamic parameters in the  
84 CEMDATA database and the experimental and mathematical methods used to obtain the  
85 parameters. Several mathematical methods to obtain thermodynamic parameters based on  
86 experimentally-determined solubility data are critically analyzed and compared. It should be  
87 noted that the methods used to determine the thermodynamic data that are necessary for adding a  
88 reaction product to CEMDATA depend on whether the chemical processes/reactions that lead to  
89 the formation of that compound are known. In cementitious systems, however, it can be difficult  
90 to know (or even hypothesize) these chemical reactions in many cases. As a result, many

assumptions might be necessary to complete the thermodynamic data; in many cases, these data might be inter-dependent, expanding the errors originating in one parameter to others. Discussion in this paper assumes that reactions that lead to the formation of the product that is being added to the CEMDATA database are known, or at the very least, can be estimated because the chemical form of the product resembles another species that is already in the CEMDATA database.

## 2. Thermodynamic data

Table 1 lists the thermodynamic parameters required to incorporate a new solid reaction product into the CEMATA database for GEMS. Since GEMS performs simulations of cementitious reactions by minimizing the Gibbs free energy of the end-members, the standard molar Gibbs free energy of formation of the new solid reaction product is needed. The Gibbs free energy of a reaction can be calculated from the measured solubility constant for the dissolution reaction of a solid phase:

$$\Delta_r G_T^0 = -RT \ln K_T \quad (1)$$

where R is the universal gas constant (8.314 J/K/mol) and  $K_T$  is the equilibrium solubility product at temperature  $T$  (K). Therefore, experimental determination of the solubility constant from dissolution (or precipitation) of a solid reaction product is typically performed to calculate the Gibbs free energy associated with the reaction. The standard thermodynamic parameters at 25 °C and 1 bar are used for entry into the CEMDATA database.[10] During the simulation, the GEMS software performs temperature and pressure corrections using the Helgeson-Kirkham-Flowers equation.[17] The Gibbs free energy of a solid phase at a specific temperature is calculated from the Gibbs free energy at standard conditions as:

$$\Delta_f G_T^0 = \Delta_f G_{T_0}^0 - (T - T_0)S_{T_0}^0 - \int_{T_0}^T \int_{T_0}^T \frac{C_p^0}{T} dT dT \quad (2)$$

As a result, values for the standard molar entropy  $S_{T_0}^0$ , enthalpy  $\Delta_f H_{T_0}^0$  and heat capacity  $C_{p,T}^0$  of the solid phase are also needed. The constant pressure heat capacity is calculated by:

$$C_{p,T}^0 = a_0 + a_1 T + a_2 T^{-2} + a_3 T^{-0.5} \quad (3)$$

where  $a_0$ ,  $a_1$ ,  $a_2$ , and  $a_3$  are empirical heat capacity parameters. Finally, molar volume of the solid reaction product is needed because GEMS also predicts the volume of each reaction product. The molar volume at standard conditions is also needed for the pressure correction of condensed substances (e.g., solids) if the simulation pressure is different from the standard state condition.[18] The approach to obtain each thermodynamic parameter is discussed in the subsequent sections.

**Table 1: List of required thermodynamic parameters of new solid reaction product**

Thermodynamic Parameter	Unit	Definition
$\log K_{S0}$	n/a	Logarithm of solubility constant at standard condition
$\Delta_f G_{T_0}^0$	kJ/mol	Standard molar Gibbs free energy of formation at standard condition

$\Delta_f H_{T_0}^0$	kJ/mol	Standard molar enthalpy of formation at standard condition
$S_{T_0}^0$	J/K/mol	Standard molar absolute entropy at standard condition
$a_0$	J/K/mol	Empirical heat capacity parameter
$a_1$	J/K <sup>2</sup> /mol	Empirical heat capacity parameter
$a_2$	J·K/mol	Empirical heat capacity parameter
$a_3$	J/K <sup>0.5</sup> /mol	Empirical heat capacity parameter
$V^0$	cm <sup>3</sup> /mol	Molar volume at standard condition

124

125 **2.1 Solubility constant**

126 Solubility of a new solid reaction product is experimentally determined at various temperatures  
 127 within the relevant temperature range of the cementitious reactions.[19–21] Suppose the  
 128 composition of the new solid phase is  $Ca_iAl_jSi_kO_l \cdot mH_2O$  and its dissolution reaction proceeds  
 129 as Eq. 4:



131 The composition of the new solid reaction product can be determined by quantifying the  
 132 component concentrations (i.e., ionic oxides composition) and bound water content of the solid.  
 133 The components in the form of ionic oxides are generally determined by XRF as the mass  
 134 percentage of each oxide in the sample.[22,23] The components can also be determined by a  
 135 combination of inductively coupled plasma-optical emission spectroscopy (ICP-OES) to obtain  
 136 major element concentrations, ICP-Mass Spectroscopy (ICP-MS) to obtain minor element  
 137 concentrations, and ion chromatography (IC) to obtain anion concentrations after digestion of the  
 138 sample.[24–28] Digestion converts solids into liquid extracts to determine the metal or anion  
 139 content. The digestion solution can be a combination of acids (e.g., nitric acid, hydrochloric acid,  
 140 hydrofluoric acid) and peroxide per standard methods [29–31] or proprietary digestion solutions  
 141 depending on the type of solid.[24] **Typically microwave radiation is used to accelerate the**  
 142 **digestion process.[30,31]** After determination of the components in the solid, the oxygen content  
 143 of the solid is quantified via stoichiometry of the corresponding oxide.

144 Bound water content of the solids can be determined by thermogravimetric analysis (TGA) under  
 145 N<sub>2</sub>. The amount of bound water is calculated from the mass loss of the sample between 105°C  
 146 and 1000 °C as recommended by RILEM TC 238-SCM.[32] However, one should be cautious  
 147 about the assumption that all evaporable water is removed at 105 °C. Some studies found  
 148 evaporable water at temperatures up to 130 °C[33]; these researchers recorded bound water mass  
 149 loss starting from 145–150 °C instead of 105 °C.[34,35] On the other hand, loss of chemically  
 150 bound water from C-S-H, AFm, and ettringite below 105 °C has been reported.[36–39] To  
 151 remove evaporable water without inducing loss of structural water below 105 °C, some studies  
 152 vacuum-filtered and equilibrated the sample at a lower temperature (e.g., 40 °C) for an hour  
 153 under N<sub>2</sub> to allow the evaporation of excess water.[24] Freeze-drying has also been proposed as a  
 154 suitable procedure; though it can still cause some change to the microstructure, it is preferred  
 155 over oven drying.[36,40,41]. Mass loss at higher temperatures can occur due to decarbonation,

156 which occurs at 600-800 °C.[42,43]. To avoid interferences in bound water measurements from  
157 decarbonation, some studies limited their TGA upper range temperatures to 500-  
158 600 °C.[19,24,44] However, whether an upper temperature lower than 1000 °C would  
159 underestimate the content of bound water is not discussed in these studies, possibly because the  
160 impact of higher temperatures on bound water content is expected to be minimal.

161 The solubility of a new solid  $Ca_iAl_jSi_kO_l \cdot mH_2O$  is experimentally determined from either  
162 dissolution or precipitation. In the dissolution approach, the synthesized dry solid is dispersed in  
163 degassed water (by boiling) and stored in plastic bottles (HDPE or PTFE).[19,20,24] The sealed  
164 bottles are then kept in suspension isothermally at several selected temperature points until the  
165 dissolution reaction reaches equilibrium as determined from statistically constant measurements  
166 of reaction products from sample aliquots measured over time. [19,45,46] The time for the  
167 dissolution reaction to reach equilibrium can vary with respect to the solid phase, temperature  
168 and solution conditions. ICP-OES is often used for analysis of major dissolution products such  
169 as Si, Al, Ca. Researchers should prepare standard sets with a matrix close to the supernatant  
170 samples from the highly saline system to ensure that the matrix effect is accounted for.[24]

171 In the precipitation approach, reacting solutions prepared using deionized, degassed water are  
172 mixed in plastic bottles to form the new solid reaction product.[20,24] **CO<sub>2</sub> will significantly  
173 interfere with cement reactions in alkaline conditions; therefore, the solution preparation,  
174 transferring, and mixing should be performed in a N<sub>2</sub>-filled glove box.** [19,20,24,47] The time  
175 for the precipitation reaction to reach equilibrium can again be determined by sampling  
176 supernatant aliquots for reactant analysis over time.[24] Once the measured aqueous  
177 concentration of metals remains stable over several (3-5) sampling events, equilibrium is  
178 assumed. However, in some cases amorphous phases can be stable for a period of time and the  
179 length of the sampling period should be sufficient to ensure that a crystalline phase has formed  
180 [48]; X-ray diffraction (XRD) can be useful in this regard.

181 After equilibrium has been obtained, the solutions are filtered through a membrane filter and  
182 acidified with HNO<sub>3</sub>. The aqueous metal content is determined by ICP-OES or ICP-MS. The  
183 type of membrane used for filtration is selected to ensure minimal adsorption of dissolved metals  
184 onto the membrane and successful capture of solids. The type and pore size of the membranes  
185 are seldom discussed in literature; however, it has been reported that measured solubility of  
186 minerals filtered through a 3kD membrane is much lower than that filtered through a 0.05 µm  
187 membrane.[49] Considering most membrane filters used in cement systems for solid-liquid  
188 separation are 0.22 or 0.45 µm in pore size,[20,47,50,51] it is possible that some fraction of small  
189 undissolved solids will pass the membrane to be measured as dissolution products. Therefore, in  
190 addition to using membranes with smaller pore size where possible, it is necessary to  
191 experimentally characterize (e.g., using nanoparticle tracking analysis) the filtrate after  
192 membrane filtration to ensure minimum presence of solids.

193 The measured aqueous metal content is then used together with speciation modeling to calculate  
194 the concentration of aqueous species to yield the solubility constant via Eq. 5:

$$195 K_{S0} = \{Ca^{2+}\}^i \cdot \{AlO_2^-\}^j \cdot \{SiO_2^0\}^k \cdot \{H_2O\}^m = (\gamma_i[Ca^{2+}])^i \cdot (\gamma_j[AlO_2^-])^j \cdot (\gamma_k[SiO_2^0])^k \cdot (\gamma_{H_2O}[H_2O])^m \quad (5)$$

196 where  $\gamma_i$  is the corresponding activity coefficient of the dissolved aqueous species. Activity  
197 coefficients of the relevant species can be calculated by various models. The Davies equation is  
198 generally valid for ionic strengths between 0.1 to 0.7 M.[52] The specific ion interaction theory  
199 (SIT) model is generally applicable up to 3-4 M.[53] At an even higher ionic strength, a more

200 complex model such as the Pitzer ion-interaction model is required.[54] In the application of  
 201 cementitious reactions, the Helgeson modification of the Truesdell-Jones version of the extended  
 202 Debye-Hückel Equation (Eq. 6) is often used and is applicable to ionic strengths up to 1-  
 203 2M:[52,55]

$$204 \log \gamma_i = \frac{-Az_i^2\sqrt{I}}{1+Ba\sqrt{I}} + bI \quad (6)$$

205 In Eq. 6,  $\gamma_i$  is the activity coefficient of ion I, A and B are Debye-Hückel solvent parameters,  $z_i$   
 206 is the ionic charge, I is the ionic strength of the solution, a is a parameter dependent on the size  
 207 of the parameter, and b is a semi-empirical parameter. In most cementitious applications, Eq. 6  
 208 has only considered a and b for the major background electrolyte (NaOH, KOH, NaCl, and  
 209 KCl).[55]

210 While the Pitzer model is seldom used for cementitious systems, it is probably the most  
 211 applicable model for alkali-activated reactions of SCMs where highly alkaline solutions (e.g., > 4  
 212 M NaOH) are generally used as the activating solution (i.e., geopolymers).[56–61] However, the  
 213 Pitzer model requires specific ion interaction parameters, which may not be available for  
 214 cementitious compositions.[62] Moreover, the Pitzer model is not directly incorporated into  
 215 GEM-Selektor, the most common geochemical software for modeling cementitious systems.[62–  
 216 64] As a result, Eq. 6 is still widely used for alkali-activated reactions despite it being only  
 217 applicable to 1-2 M.[63,65,66]

## 218 **2.2 Heat capacity**

219 As shown in Eq. 2, heat capacity is needed to calculate Gibbs free energy at a temperature  
 220 different from the standard state condition (i.e., 25 °C). The heat capacity of a solid can be  
 221 calculated via Eq. 3. While a few studies measured heat capacity experimentally using thermal  
 222 relaxation calorimetry and differential scanning calorimetry (DSC),[67,68] in the field of cement  
 223 research, the heat capacity is usually estimated using a reference reaction [20,69] or via the  
 224 additive approach of elementary oxides [47,70]. The reference reaction approach adopts heat  
 225 capacity values for solids with known heat capacity that are structurally similar to the new solid  
 226 reaction product of interest.[20,69] For example, if the unknown new solid A is structurally  
 227 similar to the aluminoferrite monosulfate (AFm) family, the reference reaction could include a  
 228 known AFm. [20,50,71]. A few examples are shown in Table 2.

229 **Table 2: Reference reactions used to calculate heat capacity based on structurally similar**  
 230 **phases**

Unknown phases	Type	Reference Reaction	Reference
Ca <sub>4</sub> Al <sub>2</sub> (OH) <sub>14</sub> ·6H <sub>2</sub> O	Hydroxy- AFm	Ca <sub>4</sub> Al <sub>2</sub> (OH) <sub>14</sub> ·6H <sub>2</sub> O + CaSO <sub>4</sub> → Ca <sub>4</sub> Al <sub>2</sub> SO <sub>4</sub> (OH) <sub>12</sub> ·6H <sub>2</sub> O + Ca(OH) <sub>2</sub>	[20]
Ca <sub>4</sub> Al <sub>2</sub> (SO <sub>4</sub> ) <sub>0.5</sub> (Cl) OH) <sub>12</sub> ·6H <sub>2</sub> O	Cl-AFm	Ca <sub>4</sub> Al <sub>2</sub> (SO <sub>4</sub> ) <sub>0.5</sub> (Cl) OH) <sub>12</sub> ·6H <sub>2</sub> O + 0.5 CaSO <sub>4</sub> → Ca <sub>4</sub> Al <sub>2</sub> SO <sub>4</sub> (OH) <sub>12</sub> ·6H <sub>2</sub> O + 0.5CaCl <sub>2</sub>	[71]

231  
 232 Because heat capacity differs greatly between free water and structurally-bound water, the  
 233 reference reaction only involves solids without free water, thus the change in heat capacity of the

234 reference reaction is approximately zero. For example, if the new solid reaction product A can be  
235 written into a reference reaction, Eq. 7:



237 where B, C, and D are species with known values of heat capacity parameters, the empirical heat  
238 capacity parameters  $a_i$  of solid A can be estimated using Eq. 8:

$$a_{i,A} = c \cdot a_{i,C} + d \cdot a_{i,D} - b \cdot a_{i,B} \quad (8)$$

240 The values of heat capacity parameters of the known species B, C, and D can be found from the  
241 built-in Nagra-PSI thermodynamic database in GEMS, the existing CEMDATA18 database, or  
242 published literature.[72,73]

243 In the additive elementary oxides approach, the heat capacity of a solid phase whose composition  
244 is  $Ca_iAl_jSi_kO_l \cdot mH_2O$  can be treated as the stoichiometric addition of heat capacity of CaO,  
245 Al<sub>2</sub>O<sub>3</sub>, SiO<sub>2</sub>, and zeolitic H<sub>2</sub>O:

$$C_{p,Ca_iAl_jSi_kO_l \cdot mH_2O}^0 = \sum \nu_i C_{p,i} \quad (9)$$

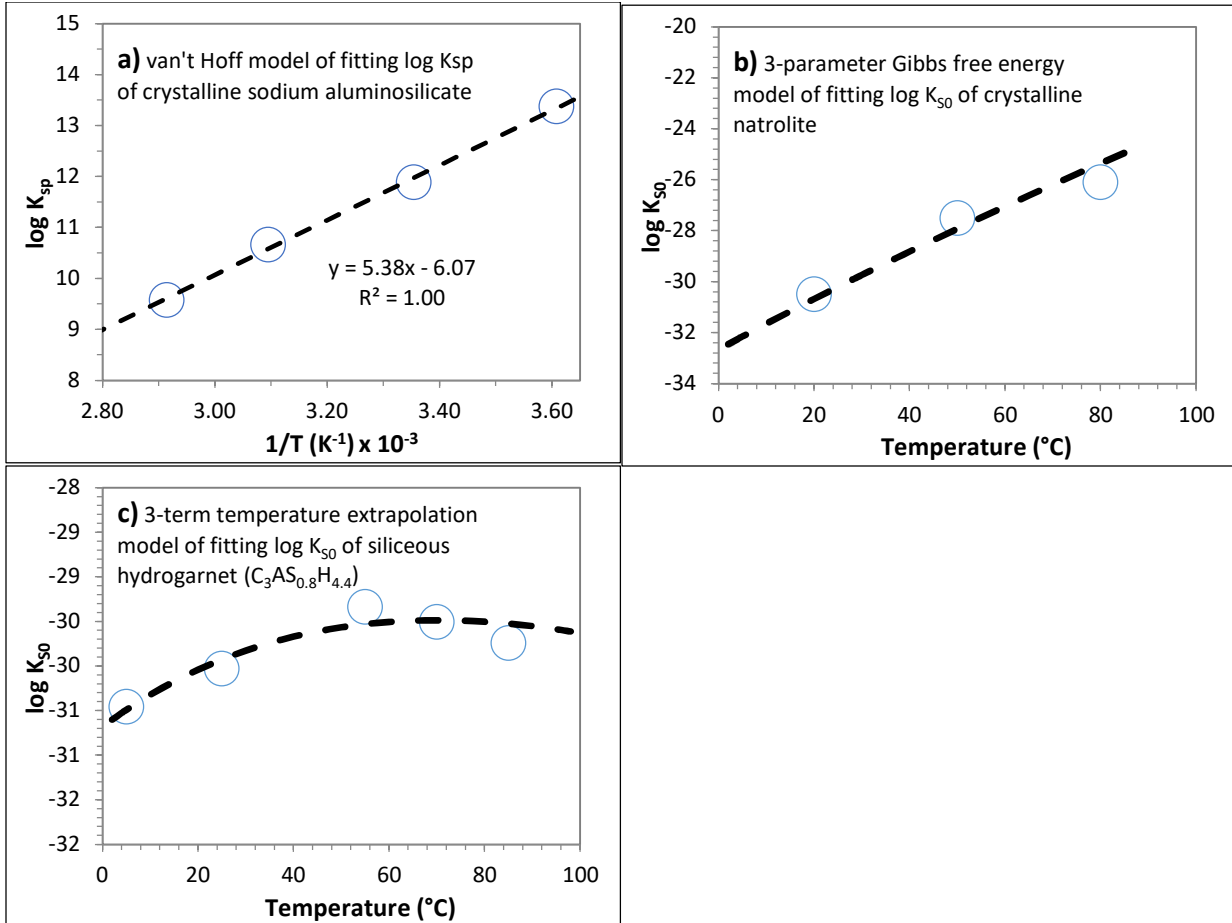
247 where  $\nu_i$  represents the stoichiometric number, and  $C_{p,i}$  is the heat capacity of the  $i$ th elementary  
248 component. Heat capacity at different **temperatures can also be** obtained by addition of heat  
249 capacities of elementary oxides at different temperatures with their stoichiometry. The  
250 temperature-heat capacity relationship obtained can be fitted to Eq. 3 to obtain the empirical heat  
251 capacity parameters  $a_i$ .

### 252 **2.3 Standard molar enthalpy, entropy, and Gibbs free energy**

253 Several methods have been used to obtain enthalpy, entropy and Gibbs free energy of formation  
254 of the solid phase depending on the level of assumptions employed.

255 **The van't Hoff model** assumes constant enthalpy of the dissolution reaction (e.g., Eq. 4) and fits  
256 the log of the solubility products at different temperature as Eq. 10. An example of using the  
257 van't Hoff model to fit solubility data of crystalline sodium aluminosilicate (N-A-S-(H)) is  
258 shown in Figure 1a. [74]

$$\log K_T = \frac{0.4343}{R} \left( \Delta_r S_{T_0}^0 - \frac{\Delta_r H_{T_0}^0}{T} \right) \quad (10)$$



260

261

**Figure 1: a) van't Hoff model of fitting solubility data of crystalline N-A-S-(H) (replotted from Williamson *et al.*, 2022)[74]; b) 3-parameter Gibbs free energy model of fitting solubility data of natrolite (replotted from Lothenbach *et al.*, 2017) [47]; and c) 3-term temperature extrapolation method of fitting solubility data of siliceous hydrogarnet (replotted from Matschei *et al.*, 2007) [20].**

267

268 By fitting Eq. 10, enthalpy and entropy of the dissolution reaction can be obtained. The obtained  
 269  $\Delta_r S_{T_0}^0$  and  $\Delta_r H_{T_0}^0$  can be used to yield the Gibbs free energy of the reaction as shown in Eq. 11:

$$270 \quad \Delta_r G_{T_0}^0 = \Delta_r H_{T_0}^0 - T_0 \Delta_r S_{T_0}^0 \quad (11)$$

271 The standard Gibbs free energy of formation,  $\Delta_f G_{T_0}^0$  for the phase is then obtained using Eq. 12 if  
 272 the known thermodynamic parameters of reactants and products are available. In the example of  
 273 a dissolution reaction shown as Eq. 4,  $\Delta_f G_{T_0}^0$  of  $Ca_iAl_jSi_kO_l \cdot mH_2O$  can be calculated as:

$$274 \quad \Delta_f G_{T_0}^0 = i \cdot \Delta_f G_{T_0, Ca^{2+}}^0 + j \cdot \Delta_f G_{T_0, AlO_4^-}^0 + k \cdot \Delta_f G_{T_0, SiO_4^{10-}}^0 + m \cdot \Delta_f G_{T_0, H_2O}^0 - \Delta_r G_{T_0}^0 \quad (12)$$

275 Similarly, the standard molar enthalpy and entropy of  $Ca_iAl_jSi_kO_l \cdot mH_2O$  are calculated using  
 276 the known standard state properties of the aqueous species:

$$277 \quad \Delta_f H_{T_0}^0 = i \cdot \Delta_f H_{T_0, Ca^{2+}}^0 + j \cdot \Delta_f H_{T_0, AlO_4^-}^0 + k \cdot \Delta_f H_{T_0, SiO_4^{10-}}^0 + m \cdot \Delta_f H_{T_0, H_2O}^0 - \Delta_r H_{T_0}^0 \quad (13)$$

278  $S_{T_0}^0 = i \cdot S_{T_0, Ca^{2+}}^0 + j \cdot S_{T_0, AlO_2^-}^0 + k \cdot S_{T_0, SiO_2^0}^0 + m \cdot S_{T_0, H_2O}^0 - \Delta_r S_{T_0}^0$  (14)

279 **The three-parameter Gibbs free energy model** fits calculated Gibbs free energy of formation  
 280 values of the phase at different temperature according to Eq. 1 and 2 [47,70,75]. The  
 281 experimentally-determined solubility products of the dissolution reaction,  $K_T$ , at different  
 282 temperature points can be used to calculate the Gibbs free energy of the dissolution reaction,  
 283  $\Delta_r G_T^0$ , at different temperatures. For the dissolution reaction shown in Eq. 4, the  $\Delta_f G_T^0$  of the new  
 284 solid phase at different temperatures can be obtained in a similar manner as employed for Eq. 12  
 285 if  $\Delta_f G_T^0$  of each aqueous species is known for a range of temperatures.

286 The heat capacity of the solid is assumed constant over the relevant temperature range; therefore,  
 287  $C_p^0$  in Eq. 2 can be treated as a constant and the equation can be integrated and simplified to yield  
 288 Eq. 15 [47,70,75]:

289 
$$\Delta_f G_T^0 = \Delta_f G_{T_0}^0 - S_{T_0}^0(T - T_0) - C_p^0 \left( T \ln \frac{T}{T_0} - T + T_0 \right)$$
 (15)

290 The heat capacity,  $C_p^0$ , and entropy,  $S_{T_0}^0$ , of the new solid phase are typically estimated using the  
 291 additivity method with the elementary oxide components [70,75,76]. This approach estimates  $C_p^0$   
 292 using Eq. 9 and estimates  $S_{T_0}^0$  using Eq. 16:

293 
$$S_{T_0, Ca_i Al_j Si_k O_l \cdot m H_2 O}^0 = \frac{\sum \nu_i S_{T_0, i}^0 (\sum \nu_i V_i^0 - V^0)}{2 \sum \nu_i V_i^0}$$
 (16)

294 where  $\nu_i$  represents the stoichiometric number,  $S_{T_0, i}^0$  is the standard molar entropy, and  $V_i^0$  is the  
 295 molar volume of the  $i$ th elementary components;  $V^0$  is the molar volume of the new solid phase.  
 296 While this approach is useful for crystalline phases, its use in estimating  $C_p^0$  and  $S_{T_0}^0$  for  
 297 amorphous phases may be limited as  $C_p^0$  and  $S_{T_0}^0$  values of amorphous elementary oxides are  
 298 generally not available.

299 The standard molar Gibbs free energy of formation,  $\Delta_f G_{T_0}^0$  can be obtained by fitting the Gibbs  
 300 free energies of formation for a range of temperatures using Eq. 15. An example of using the  
 301 three-parameter Gibbs free energy model to fit the solubility data of natrolite is shown in Figure  
 302 1b. [47]

303 **The three-term temperature extrapolation model** assumes the heat capacity of the dissolution  
 304 reaction  $\Delta_r C_p_T^0$  is constant over the relevant temperature range and fits the 3-term equation  
 305 shown in Eq. 17: [77,78]

306 
$$\log K_T = A_0 + A_2 T^{-1} + A_3 \ln T$$
 (17)

307 The relationship of thermodynamic parameters and the “ $\log K$ ” function shown in Eqs. 18 to 20  
 308 are then used to obtain the thermodynamic parameters of the dissolution reaction:[8,20]

309 
$$A_0 = \frac{0.4343}{R} [\Delta_r S_{T_0}^0 - \Delta_r C_p_{T_0}^0 (1 + \ln T_0)]$$
 (18)

310 
$$A_2 = -\frac{0.4343}{R} (\Delta_r H_{T_0}^0 - \Delta_r C_p_{T_0}^0 T_0)$$
 (19)

311 
$$A_3 = \frac{0.4343}{R} \Delta_r C_p_{T_0}^0 T_0$$
 (20)

312 The molar entropy of the reaction,  $\Delta_r S_{T_0}^0$ , and the molar enthalpy of the reaction,  $\Delta_r H_{T_0}^0$ , are  
313 estimated from Eq. 18 and 19, respectively, by regression of the “*logK*” function in Eq. 17. The  
314 heat capacity of the reaction,  $\Delta_r Cp_{T_0}^0 T_0$ , is generally not fitted using Eq. 20; rather, it is estimated  
315 from reference reactions as discussed in section 2.2.[8,20] The Gibbs free energy of the reaction  
316 can be obtained from Eq. 11, and the standard Gibbs free energy of formation,  $\Delta_f G_{T_0}^0$  for the new  
317 solid phase is then obtained using Eq. 12. The standard molar **enthalpy of formation**  $\Delta_f H_{T_0}^0$  and  
318 entropy  $S_{T_0}^0$  of the new solid phase  $Ca_iAl_jSi_kO_l \cdot mH_2O$  are calculated using Eq. 13 and 14. An  
319 example of using the three-term temperature extrapolation model to fit the solubility data of  
320 siliceous hydrogarnet is shown in Figure 1c. [20]

## 321 **2.4 Molar volume**

322 Molar volume of the new solid reaction product phase is needed so that the simulation can  
323 predict the volume fraction of the formed phases and thus porosity of the cementitious system.  
324 The molar volume  $V^0$  is calculated by dividing the molecular weight  $MW$  by the density  $\rho$  of the  
325 solid phase as shown in Eq. 21:

$$326 \quad V^0 = \frac{MW}{\rho} \quad (21)$$

327 One common technique to obtain the density of the new solid is gas pycnometry using helium  
328 gas.[51,79–81] This method measures the pressure change resulting from displacement of helium  
329 by the solid. After drying, the pre-weighed solid sample is placed into the pycnometer to obtain  
330 the density of the solid sample.[51]

331 When the new solid of interest is crystalline, the density of the new solid can also be estimated  
332 from crystallographic data and unit cell constants determined by XRD.[82,83] However, if the  
333 cement reaction product of interest is amorphous, XRD techniques are of limited use to  
334 determine the density of such solids.

335

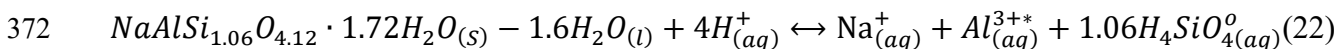
## 336 **3. Discussion**

337 The three-parameter Gibbs free energy model and the three-term temperature extrapolation  
338 model as described in Section 2 have been widely used to expand CEMDATA over the past few  
339 decades.[8,20,47,50,69,84] The van’t Hoff model has been used in some recent studies.[45,74]  
340 By limiting the needed experimental work for solubility measurements at different temperatures,  
341 these three methods provide a relatively straightforward framework to incorporate new reaction  
342 products into the CEMDATA database. Nevertheless, researchers need to be aware of some  
343 intrinsic assumptions of these methods with respect to obtaining molar enthalpy, entropy, and  
344 Gibbs free energy.

345 All three methods to obtain molar enthalpy, entropy, and Gibbs free energy are based on fitting  
346 experimentally-determined  $K_T$  values. Both the three-parameter Gibbs free energy model and the  
347 three-term temperature extrapolation method require estimation of the heat capacity. In the three-  
348 parameter model, while estimating heat capacity and entropy from elementary oxides yields  
349 satisfactory results for crystalline phases, such estimation cannot be performed when the phase of  
350 interest is amorphous, as heat capacity or entropy values for amorphous elementary oxides are  
351 difficult to obtain. In the three-term extrapolation model, the estimated heat capacity based on  
352 Eq. 7 and 8 requires the minerals in the reference reaction to be structurally similar to the new

353 solid to allow the heat capacity of the reference reaction  $\Delta_r Cp_T^0$  to be approximately zero.  
 354 However, previous research has not set forth a systematic method for selecting the reference  
 355 reaction, the only guidance is that known components from structurally similar phases to the new  
 356 solid should be used and the importance of selecting a reference reaction without free water has  
 357 been highlighted.[20,71] This assumption that  $\Delta_r Cp_T^0$  is zero for the reference reaction risks error  
 358 in determination of the heat capacity if  $\Delta_r Cp_T^0$  of the reference reaction is not zero. In addition,  
 359 the three-term extrapolation fitting procedure for enthalpy and entropy employing Equations 17-  
 360 20 is somewhat circular because Equations 18-20 include fitting the reaction heat capacity term.

361 The van't Hoff approach, on the other hand, assumes constant enthalpy of the dissolution  
 362 reaction which may be applicable over a small temperature range where the change in heat  
 363 capacity of the dissolution reaction is negligible. A demonstration of using the van't Hoff model  
 364 and the three-parameter Gibbs free energy model is provided here and shows that the simpler  
 365 van't Hoff approach is sufficient for the relevant temperature range of cement hydration.[74] In  
 366 this example, crystalline N-A-S-(H) samples were synthesized using sodium silicate and sodium  
 367 aluminate solutions across a range of bulk aqueous Si/Al ratios at different temperatures  
 368 following the precipitation approach discussed in Section 2.1. Concentrations of sodium,  
 369 aluminum, and silica in the supernatants were measured, activities were calculated using  
 370 PHREEQC and solubility constants were calculated following the N-A-S-(H) dissolution  
 371 reaction shown in Eq. 22 in a similar manner as Eq. 5.



373 Both the van't Hoff model and the three-parameter Gibbs free energy model were used to  
 374 calculate thermodynamic parameters as shown in Table 3. The van't Hoff expression yielded  
 375 similar Gibbs free energy of formation data as the three-parameter Gibbs free energy model.  
 376 Thus, the van't Hoff approach may obviate the need for estimating the heat capacity from  
 377 elementary oxide addition or reference reactions over reasonably small temperature ranges.  
 378 However, one limitation of using a small temperature range is that the regression is not very  
 379 sensitive to the value of entropy.[74]

380 **Table 3: Thermodynamic parameters of crystalline N-A-S-(H) calculated from three-  
 381 parameter Gibbs free energy model and van't Hoff model.**

	Parameters of N-A-S-(H) phases			
	$\Delta_f H_{T_0}^0$ (kJ/mol)	$S_{T_0}^0$ (J/mol·K)	$\Delta_f G_{T_0}^0$ (kJ/mol)	$c_{p,T_0}^0$ (J/mol·K)
three-parameter	-2657.1	208.2	-2443.9	203.2
van't Hoff	-2674.2	152.7	-2444.5	281.6

382

#### 383 4. Recommendation

384 Calculation of thermodynamic parameters are based on regressions of  $K_T$ . To mitigate the error  
 385 in  $K_T$  based on measured concentrations, determining  $K_T$  for at least 4 or 5 temperature points is  
 386 recommended. Experimental validation of thermodynamic parameters that are currently fitted or  
 387 calculated is also recommended as discussed next.

388 Heat capacity of dry powders can be experimentally determined by thermal relaxation  
 389 calorimetry and DSC.[67,68,85] Recently, the physical property measurement system (PPMS), a

390 commercially available automated relaxation calorimeter , has been used to determine the heat  
391 capacity of solids.[86,87] By heating a mass of new solid in the PPMS or DSC over a  
392 temperature range, the heat capacity of the new solid can be calculated as: [88]

393 
$$C_{p,T}^0 = \frac{M_{TH}}{m/MW} \quad (23)$$

394 where  $M_{TH}$  is the measured thermal mass (J/K),  $m$  is mass of the solid sample (g), and  $MW$  is  
395 the molecular weight of the solid of interest. Nevertheless, limited studies have employed  
396 calorimetry techniques to determine heat capacity of cementitious reaction products.[67,85] Most  
397 studies still estimate heat capacity based on the methods described in Section 2. It is  
398 recommended that when the pure phase composition of the reaction products is known and  
399 advanced calorimetry techniques are available for heat capacity measurements, experimentally  
400 determine heat capacities should be obtained and compared to values determined from a  
401 reference equation or addition of elementary oxides. Not only will the experimentally  
402 determined data improve the accuracy of the thermodynamic parameter estimates, but the data  
403 will also help to validate the other estimation methods.

404 When the enthalpy of the reaction needs to be experimentally determined, solution calorimetry is  
405 used.[85,89,90] In this technique, the new solid is dissolved in a suitable solvent (e.g., 5N HCl)  
406 and the heat released or consumed is recorded. The measured heat from the acid dissolution is  
407 then used with known or measured heat release data from reference compounds to obtain  $\Delta_f H_{T_0}^0$   
408 of the new solid.[85] However, accuracy of measured  $\Delta_r H_{T_0}^0$  values for the dissolution reaction  
409 can be impacted by the presence of impurities in the synthesized new solid.[69] Therefore, use of  
410 experimentally-determined enthalpy values should also be employed with caution.

411 To validate estimated entropy values from fitting or calculation, experimentally-determined  
412 entropy values can be calculated from the measured heat capacity over a range of temperatures  
413 and under constant pressure as shown in Eq. 24.[91,92] However, determination of entropy from  
414 heat capacity measurement is hardly used for cement reaction products.[93]

415 
$$\Delta S_T^0 = \Delta S_{T=0}^0 + \int_0^T \frac{C_{p,T}^0}{T} dT \quad (24)$$

416

## 417 **5. Conclusion**

418 In summary, thermodynamic modeling is a valuable tool in the study of cementitious reactions  
419 with new SCMs if used with an accurate and complete database. Expanding the current database  
420 to include more solid reaction products that arise with the use of new SCMs will be the focus of  
421 future efforts. Estimation of thermodynamic parameters based on measured solubility products at  
422 several temperatures is a well established approach and has been widely used in many studies to  
423 expand the CEMDATA database. Nevertheless, this widely used framework of methods involves  
424 assumptions that might need further improvement when being extended to new reaction products  
425 of cementitious reactions.

426

## 427 **Acknowledgments**

428 The authors thank Advanced Research Projects Agency–Energy (ARPA-E) Grant DE-AR0001143  
429 and National Science Foundation (NSF) Award CMMI-1903457 for financial support of the study  
430 presented in this paper.

431  
432 **Authorship Statement**  
433 Tongren Zhu: Conceptualization, Investigation, Writing – original draft  
434 Maria Juenger: Conceptualization, Writing – review and editing, Supervision, Funding acquisition  
435 O. Burkan Isgor: Conceptualization, Writing – review and editing, Funding acquisition  
436 Lynn Katz: Conceptualization, Writing – review and editing, Supervision, Funding acquisition  
437

438 **References**  
439 [1] A. Hasanbeigi, L. Price, E. Lin, Emerging energy-efficiency and CO<sub>2</sub> emission-reduction  
440 technologies for cement and concrete production: A technical review, *Renewable and Sustainable*  
441 *Energy Reviews.* 16 (2012) 6220–6238.  
442 [2] L. Barcelo, J. Kline, G. Walenta, E. Gartner, Cement and carbon emissions, *Materials and*  
443 *Structures/Materiaux et Constructions.* 47 (2014) 1055–1065.  
444 [3] T.R. Naik, R. Kumar, Sustainable concrete with industrial and postconsumer by-product materials,  
445 in: *Second International Conference on Sustainable Construction Materials and Technologies,*  
446 *Ancona, Italy, June 28-30, 2010, 2010.*  
447 [4] C. Meyer, The greening of the concrete industry, *Cem Concr Compos.* 31 (2009) 601–605.  
448 [5] K. Bharadwaj, R.M. Ghantous, F. Sahan, O.B. Isgor, W.J. Weiss, Predicting pore volume,  
449 compressive strength, pore connectivity, and formation factor in cementitious pastes containing fly  
450 ash, *Cem Concr Compos.* 122 (2021) 104113.  
451 [6] K. Bharadwaj, O.B. Isgor, W.J. Weiss, K.S.T. Chopperla, A. Choudhary, G.D. Vasudevan, D.  
452 Glosser, J.H. Ideker, D. Trejo, A New Mixture Proportioning Method for Performance- Based  
453 Concrete, *Materials Journal.* 119 (2022) 207–220.  
454 [7] B. Lothenbach, F. Winnefeld, Thermodynamic modelling of the hydration of Portland cement,  
455 *Cem Concr Res.* 36 (2006) 209–226.  
456 [8] D. Damidot, B. Lothenbach, D. Herfort, F.P. Glasser, Thermodynamics and cement science, *Cem*  
457 *Concr Res.* 41 (2011) 679–695.  
458 [9] B. Lothenbach, M. Zajac, Application of thermodynamic modelling to hydrated cements, *Cem*  
459 *Concr Res.* 123 (2019) 105779.  
460 [10] B. Lothenbach, D.A. Kulik, T. Matschei, M. Balonis, L. Baquerizo, B. Dilnesa, G.D. Miron, R.J.  
461 Myers, *Cemdata18: A chemical thermodynamic database for hydrated Portland cements and*  
462 *alkali-activated materials,* *Cem Concr Res.* 115 (2019) 472–506.  
463 [11] D.L. Parkhurst, C.A.J. Appelo, Description of input and examples for PHREEQC version 3—A  
464 computer program for speciation, batch-reaction, one-dimensional transport, and inverse  
465 geochemical calculations: U.S. Geological Survey Techniques and Methods, book 6, chap. A43,  
466 2013. <https://pubs.usgs.gov/tm/06/a43/>.

467 [12] D. Kulik, U. Berner, E. Curti, Modelling Chemical Equilibrium Partitioning with the GEMS-PSI  
468 Code, Paul Scherrer Institut Scientific Report Volume IV, CH-5232 Villigen PSI (Switzerland),  
469 2003.

470 [13] A.M.M. Leal, D.A. Kulik, W.R. Smith, M.O. Saar, An overview of computational methods for  
471 chemical equilibrium and kinetic calculations for geochemical and reactive transport modeling, in:  
472 Pure and Applied Chemistry, Walter de Gruyter GmbH, 2017: pp. 597–643.

473 [14] W.R. Smith, R.W. Missen, Chemical Reaction Equilibrium Analysis: Theory and Algorithms,  
474 John Wiley, New York, 1983.

475 [15] N. Holmes, M. Tyrer, R. West, A. Lowe, D. Kelliher, Using PHREEQC to model cement  
476 hydration, Constr Build Mater. 319 (2022).

477 [16] D.A. Kulik, T. Wagner, S. V. Dmytrieva, G. Kosakowski, F.F. Hingerl, K. V. Chudnenko, U.R.  
478 Berner, GEM-Selektor geochemical modeling package: Revised algorithm and GEMS3K  
479 numerical kernel for coupled simulation codes, Comput Geosci. 17 (2013) 1–24.

480 [17] D.A. Sverjensky, E.L. Shock, H.C. Helgeson, Prediction of the thermodynamic properties of  
481 aqueous metal complexes to 1000°C and 5 kb, Geochim Cosmochim Acta. 61 (1997) 1359–1412.

482 [18] GEMS Development Team, GEMS3 Theory TD Calculations, (n.d.).  
483 [http://gems.web.psi.ch/TDB/doc/html/theory\\_tdb.html](http://gems.web.psi.ch/TDB/doc/html/theory_tdb.html) (accessed June 4, 2020).

484 [19] B.Z. Dilnesa, B. Lothenbach, G. Renaudin, A. Wichser, D. Kulik, Synthesis and characterization  
485 of hydrogarnet  $\text{Ca}_3(\text{Al}_x\text{Fe}_1-x)\text{Si}_2\text{O}_4\text{y}(\text{OH})_{4(3-y)}$ , Cem Concr Res. 59 (2014) 96–111.

486 [20] T. Matschei, B. Lothenbach, F.P. Glasser, Thermodynamic properties of Portland cement hydrates  
487 in the system  $\text{CaO}\text{-}\text{Al}_2\text{O}_3\text{-}\text{SiO}_2\text{-}\text{CaSO}_4\text{-}\text{CaCO}_3\text{-}\text{H}_2\text{O}$ , Cem Concr Res. 37 (2007) 1379–1410.

488 [21] T. Schmidt, B. Lothenbach, M. Romer, K. Scrivener, D. Rentsch, R. Figi, A thermodynamic and  
489 experimental study of the conditions of thaumasite formation, Cem Concr Res. 38 (2008) 337–  
490 349.

491 [22] P. Stutzman, A. Heckert, NIST TN-1816: Performance Criteria For an ASTM XRF Standard Test  
492 Method For Chemical Analysis of Hydraulic Cements: Inter-Laboratory Study on Cements A and  
493 B, 2013.

494 [23] P. Wedding, B. Wheeler, Chemical Analysis of Portland Cement by Energy Dispersive X-Ray  
495 Fluorescence, Cement, Concrete and Aggregates. 5 (1983) 123.

496 [24] T. Williamson, J. Han, L. Katz, G. Sant, M. Juenger, Method for experimentally determining N-A-  
497 S-(H) solubility, RILEM Technical Letters. 3 (2019) 104–113.

498 [25] W. Devos, C. Moor, Determination of 14 trace element concentrations in two Dillinger  
499 Hüttenwerke Portland cement reference materials by sector field and quadrupole ICP-MS, J Anal  
500 At Spectrom. 17 (2002) 138–141.

501 [26] S.S. Potgieter, L. Marjanovic, A further method for chloride analysis of cement and cementitious  
502 materials - ICP-OES, Cem Concr Res. 37 (2007) 1172–1175.

503 [27] U.R. Funteas, J.A. Wallace, F.W. Fochtman, A Comparative Analysis Of Mineral Trioxide  
504 Aggregate And Portland Cement, Australian Endodontic Journal. 29 (2003) 43–44.

505 [28] Y.L. Wei, C.L. Cheng, Determination of total Cl in incinerator fly ashes utilized as cement raw  
506 materials, Constr Build Mater. 124 (2016) 544–549.

507 [29] USEPA, “Method 3050B: Acid Digestion of Sediments, Sludges, and Soils,” Revision 2,  
508 Washington, DC, 1996. <https://www.epa.gov/sites/production/files/2015-06/documents/epa-3050b.pdf>.

510 [30] USEPA, "Method 3051A (SW-846): Microwave Assisted Acid Digestion of Sediments, Sludges,  
511 and Oils," Revision 1, Washington, DC, 2007. <https://www.epa.gov/sites/production/files/2015-12/documents/3051a.pdf>.

513 [31] USEPA, "Method 3052 (SW-846): Microwave Assisted Acid Digestion of Siliceous and  
514 Organically Based Matrices," Revision 0, Washington, DC, 1996.  
515 <https://www.epa.gov/sites/production/files/2015-12/documents/3052.pdf>.

516 [32] K.L. Scrivener, B. Lothenbach, N. De Belie, E. Gruyaert, J. Skibsted, R. Snellings, A. Vollpracht,  
517 TC 238-SCM: hydration and microstructure of concrete with SCMs: State of the art on methods to  
518 determine degree of reaction of SCMs, *Mater Struct.* 48 (2015) 835–862.

519 [33] S. Kourounis, S. Tsivilis, P.E. Tsakiridis, G.D. Papadimitriou, Z. Tsibouki, Properties and  
520 hydration of blended cements with steelmaking slag, *Cem Concr Res.* 37 (2007) 815–822.

521 [34] J.I. Escalante-Garcia, Nonevaporable water from neat OPC and replacement materials in  
522 composite cements hydrated at different temperatures, *Cem Concr Res.* 33 (2003) 1883–1888.

523 [35] P. Mounanga, A. Khelidj, A. Loukili, V. Baroghel-Bouny, Predicting Ca(OH)2 content and  
524 chemical shrinkage of hydrating cement pastes using analytical approach, *Cem Concr Res.* 34  
525 (2004) 255–265.

526 [36] C. Gallé, Effect of drying on cement-based materials pore structure as identified by mercury  
527 intrusion porosimetry - A comparative study between oven-, vacuum-, and freeze-drying, *Cem  
528 Concr Res.* 31 (2001) 1467–1477.

529 [37] J. Zhang, G.W. Scherer, Comparison of methods for arresting hydration of cement, *Cem Concr  
530 Res.* 41 (2011) 1024–1036.

531 [38] D. Snoeck, L.F. Velasco, A. Mignon, S. Van Vlierberghe, P. Dubrule, P. Lodewyckx, N. De Belie,  
532 The influence of different drying techniques on the water sorption properties of cement-based  
533 materials, *Cem Concr Res.* 64 (2014) 54–62.

534 [39] L. Zhang, F.P. Glasser, Critical examination of drying damage to cement pastes, *Advances in  
535 Cement Research.* 12 (2000) 79–88.

536 [40] J. Zhang, G.W. Scherer, Comparison of methods for arresting hydration of cement, *Cem Concr  
537 Res.* 41 (2011) 1024–1036.

538 [41] A. Korpa, R. Trettin, The influence of different drying methods on cement paste microstructures  
539 as reflected by gas adsorption: Comparison between freeze-drying (F-drying), D-drying, P-drying  
540 and oven-drying methods, *Cem Concr Res.* 36 (2006) 634–649.

541 [42] W. Deboucha, N. Leklou, A. Khelidj, M.N. Oudjit, Hydration development of mineral additives  
542 blended cement using thermogravimetric analysis (TGA): Methodology of calculating the degree  
543 of hydration, *Constr Build Mater.* 146 (2017) 687–701.

544 [43] I. Pane, W. Hansen, Investigation of blended cement hydration by isothermal calorimetry and  
545 thermal analysis, *Cem Concr Res.* 35 (2005) 1155–1164.

546 [44] C. Gosselin, K.L. Scrivener, Microstructure development of calcium aluminate cement accelerated  
547 with lithium sulphate, in: *Calcium Aluminate Cements: Proceedings of the Centenary Conference,*  
548 Avignon, June 30-July 2, 2008, 2008.

549 [45] L. Gomez-Zamorano, M. Balonis, B. Erdemli, N. Neithalath, G. Sant, C–(N)–S–H and N–A–S–H  
550 gels: Compositions and solubility data at 25°C and 50°C, *Journal of the American Ceramic  
551 Society.* 100 (2017) 2700–2711.

552 [46] B. Walkley, X. Ke, O. Hussein, J.L. Provis, Thermodynamic properties of sodium aluminosilicate  
553 hydrate (N-A-S-H), *Dalton Transactions*. 50 (2021) 13968–13984.

554 [47] B. Lothenbach, E. Bernard, U. Mäder, Zeolite formation in the presence of cement hydrates and  
555 albite, *Physics and Chemistry of the Earth*. 99 (2017) 77–94.

556 [48] T. Williamson, L.E. Katz, J. Han, H.A. Dobbs, B.F. Chmelka, G. Sant, M.C.G. Juenger,  
557 Relationship between aqueous chemistry and composition, structure, and solubility of sodium  
558 aluminosilicate hydrates, *Journal of the American Ceramic Society*. 103 (2020) 2160–2172.

559 [49] A. Mendoza-Flores, M. Villalobos, T. Pi-Puig, N.V. Martínez-Villegas, Revised aqueous  
560 solubility product constants and a simple laboratory synthesis of the Pb(II) hydroxycarbonates:  
561 Plumbonacrite and hydrocerussite, *Geochem J.* 51 (2017) 315–328.

562 [50] B. Lothenbach, L. Pelletier-Chaignat, F. Winnefeld, Stability in the system CaO-Al<sub>2</sub>O<sub>3</sub>-H<sub>2</sub>O,  
563 *Cem Concr Res.* 42 (2012) 1621–1634.

564 [51] L. Gomez-Zamorano, M. Balonis, B. Erdemli, N. Neithalath, G. Sant, C-(N)-S-H and N-A-S-H  
565 gels: Compositions and solubility data at 25°C and 50°C, *Journal of the American Ceramic  
566 Society*. 100 (2017) 2700–2711.

567 [52] T. Wagner, D.A. Kulik, F.F. Hingerl, S. V. Dmytrievava, Gem-selektor geochemical modeling  
568 package: TSolMod library and data interface for multicomponent phase models, *Can Mineral.* 50  
569 (2012) 1173–1195.

570 [53] Y. Xiong, Estimation of medium effects on equilibrium constants in moderate and high ionic  
571 strength solutions at elevated temperatures by using specific interaction theory (SIT): Interaction  
572 coefficients involving Cl, OH- and Ac- up to 200°C and 400 bars, *Geochem Trans.* 7 (2006) 1–19.

573 [54] K.S. Pitzer, Characteristics of very concentrated aqueous solutions, *Physics and Chemistry of the  
574 Earth*. 13–14 (1981) 249–272.

575 [55] H.C. Helgeson, D.H. Kirkham, G.C. Flowers, Theoretical prediction of the thermodynamic  
576 behavior of aqueous electrolytes at high pressures and temperatures: IV. Calculation of activity  
577 coefficients, osmotic coefficients, and apparent molal and standard and relative partial molal  
578 properties to 600°C and 5 kb., *Am J Sci.* 281 (1981) 1249–1516.

579 [56] M. Ben Haha, G. Le Saout, F. Winnefeld, B. Lothenbach, Influence of activator type on hydration  
580 kinetics, hydrate assemblage and microstructural development of alkali activated blast-furnace  
581 slags, *Cem Concr Res.* 41 (2011) 301–310.

582 [57] F. Puertas, S. Martínez-Ramírez, S. Alonso, T. Vázquez, Alkali-activated fly ash/slag cements.  
583 Strength behaviour and hydration products, *Cem Concr Res.* 30 (2000) 1625–1632.

584 [58] T. Williamson, M.C.G. Juenger, The role of activating solution concentration on alkali-silica  
585 reaction in alkali-activated fly ash concrete, *Cem Concr Res.* 83 (2016) 124–130.

586 [59] S. Alonso, A. Palomo, Calorimetric study of alkaline activation of calcium hydroxide-metakaolin  
587 solid mixtures, *Cem Concr Res.* 31 (2001) 25–30.

588 [60] W. Rakngan, T. Williamson, R.D. Ferron, G. Sant, M.C.G. Juenger, Controlling workability in  
589 alkali-activated Class C fly ash, *Constr Build Mater.* 183 (2018) 226–233.

590 [61] X. Guo, H. Shi, W.A. Dick, Compressive strength and microstructural characteristics of class C fly  
591 ash geopolymer, *Cem Concr Compos.* 32 (2010) 142–147.

592 [62] D. Prentice, S. Bernal, M. Bankhead, M. Hayes, J. Provis, Using the Pitzer Model to Predict  
593 Aqueous Solution Compositions of Portland Cements Blended with Supplementary Cementitious

594 Materials, in: Proceedings of International Conferences (ICACMS) Advances in Construction  
595 Materials and Systems Vol 2, RILEM Publications SARL, 2017: pp. 638–647.

596 [63] M.U. Okoronkwo, M. Balonis, L. Katz, M. Juenger, G. Sant, A thermodynamics-based approach  
597 for examining the suitability of cementitious formulations for solidifying and stabilizing coal-  
598 combustion wastes, *J Environ Manage.* 217 (2018) 278–287.

599 [64] D. Prentice, Thermodynamic modelling of ultra-long-term durability of cementitious binders for  
600 waste immobilisation, PhD Dissertation, The University of Sheffield, 2018.

601 [65] R.J. Myers, B. Lothenbach, S.A. Bernal, J.L. Provis, Thermodynamic modelling of alkali-  
602 activated slag cements, *Applied Geochemistry.* 61 (2015) 233–247.

603 [66] R.J. Myers, S.A. Bernal, J.L. Provis, A thermodynamic model for C-(N)-A-S-H gel: CNASH-ss.  
604 Derivation and validation, *Cem Concr Res.* 66 (2014) 27–47.

605 [67] J. Ederová, V. Šatava, Heat capacities of C3AH6, C4A $\bar{S}$ H12 and C6A $\bar{S}$ 3H32, *Thermochim Acta.*  
606 31 (1979) 126–128.

607 [68] C.A. Geiger, E. Dachs, A. Benisek, Thermodynamic behavior and properties of katoite  
608 (hydrogrossular): A calorimetric study, *American Mineralogist.* 97 (2012) 1252–1255.

609 [69] P. Blanc, X. Bourbon, A. Lassin, E.C. Gaucher, Chemical model for cement-based materials:  
610 Thermodynamic data assessment for phases other than C-S-H, *Cem Concr Res.* 40 (2010) 1360–  
611 1374.

612 [70] B. Ma, B. Lothenbach, Synthesis, characterization, and thermodynamic study of selected Na-based  
613 zeolites, *Cem Concr Res.* 135 (2020) 106111.

614 [71] M. Balonis, The influence of inorganic chemical accelerators and corrosion inhibitors on the  
615 mineralogy of hydrated Portland Cement Systems (PhD Dissertation), University of Aberdeen,  
616 Aberdeen, United Kingdom, 2010.

617 [72] T. Thoenen, D. Kulik, Nagra/PSI Chemical Thermodynamic Data Base 01/01 for the GEM-  
618 Selektor (V.2-PSI) Geochemical Modeling Code: Release 28-02-03. Internal Report TM-44-03-  
619 04, 2003.

620 [73] T. Thoenen, W. Hummel, U. Berner, E. Curti, The PSI/Nagra Chemical Thermodynamic Database  
621 12/07, PSI Report 14-04, Villigen PSI, Switzerland, 2014.

622 [74] T. Williamson, T. Zhu, J. Han, G. Sant, O.B. Isgor, L. Katz, M. Juenger, Effect of Temperature on  
623 N-A-S-(H) Composition, Solubility, and Structure, In Preparation. (n.d.).

624 [75] B. Ma, B. Lothenbach, Synthesis, characterization, and thermodynamic study of selected K-based  
625 zeolites, *Cem Concr Res.* 148 (2021).

626 [76] H.C. Helgeson, J.M. Delany, W.H. Nesbitt, D.K. Bird, Summary and critique of the  
627 thermodynamic properties of rock-forming minerals, *Am J Sci.* 278-A (1978) 1–229.

628 [77] D.A. Kulik, Thermodynamic properties of surface species at the mineral-water interface under  
629 hydrothermal conditions: A gibbs energy minimization single-site 2pK(A) triple-layer model of  
630 rutile in NaCl electrolyte to 250°C, *Geochim Cosmochim Acta.* 64 (2000) 3161–3179.

631 [78] D.A. Kulik, Kulik, D. A. (2002). Minimising uncertainty induced by temperature extrapolations of  
632 thermodynamic data: a pragmatic view on the integration of thermodynamic databases into  
633 geochemical computer codes., in: *The Use of Thermodynamic Databases in Performance*  
634 *Assessment*, Barcelona, Spain, 2002: pp. 125–137.

635 [79] J. Shekhovtsova, I. Zhernovsky, M. Kovtun, N. Kozhukhova, I. Zhernovskaya, E. Kearsley,  
636 Estimation of fly ash reactivity for use in alkali-activated cements - A step towards sustainable  
637 building material and waste utilization, *J Clean Prod.* 178 (2018) 22–33.

638 [80] M. Sadique, H. Al-Nageim, W. Atherton, L. Seton, N. Dempster, Mechano-chemical activation of  
639 high-Ca fly ash by cement free blending and gypsum aided grinding, *Constr Build Mater.* 43  
640 (2013) 480–489.

641 [81] R.F. Feldman, Helium flow and density measurement of the hydrated tricalcium silicate - water  
642 system, *Cem Concr Res.* 2 (1972) 123–136.

643 [82] M. Balonis, F.P. Glasser, The density of cement phases, *Cem Concr Res.* 39 (2009) 733–739.

644 [83] I.G. Richardson, The calcium silicate hydrates, *Cem Concr Res.* 38 (2008) 137–158.

645 [84] M. Balonis, B. Lothenbach, G. le Saout, F.P. Glasser, Impact of chloride on the mineralogy of  
646 hydrated Portland cement systems, *Cem Concr Res.* 40 (2010) 1009–1022.

647 [85] F. Bellmann, J. Majzlan, K.D. Grevel, E. Dachs, H.M. Ludwig, Analysis of thermodynamic data  
648 of calcium aluminate monocarbonate hydrate, *Cem Concr Res.* 116 (2019) 89–94.

649 [86] J.C. Lashley, M.F. Hundley, A. Migliori, J.L. Sarrao, P.G. Pagliuso, T.W. Darling, M. Jaime, J.C.  
650 Cooley, W.L. Hults, L. Morales, D.J. Thoma, J.L. Smith, J. Boerio-Goates, B.F. Woodfield, G.R.  
651 Stewart, R.A. Fisher, N.E. Phillips, Critical examination of heat capacity measurements made on a  
652 quantum design physical property measurement system, *Cryogenics (Guildf).* 43 (2003) 369–378.

653 [87] Q. Shi, C.L. Snow, J. Boerio-Goates, B.F. Woodfield, Accurate heat capacity measurements on  
654 powdered samples using a Quantum Design physical property measurement system, *Journal of  
655 Chemical Thermodynamics.* 42 (2010) 1107–1115.

656 [88] A. Jayalath, R. San Nicolas, M. Sofi, R. Shanks, T. Ngo, L. Aye, P. Mendis, Properties of  
657 cementitious mortar and concrete containing micro-encapsulated phase change materials, *Constr  
658 Build Mater.* 120 (2016) 408–417.

659 [89] C.J.M. Houtepen, H.N. Stein, The enthalpies of formation and of dehydration of some AFm  
660 phases with singly charged anions, *Cem Concr Res.* 6 (1976) 651–658.

661 [90] H.A. Berman, E.S. Newman, Heat of formation of calcium aluminate monosulfate at 25 °C, *J Res  
662 Natl Bur Stand A Phys Chem.* 67A (1963) 1–13.

663 [91] W. Yong, E. Dachs, A. Benisek, R.A. Secco, Heat capacity, entropy and phase equilibria of  
664 stishovite, *Phys Chem Miner.* 39 (2012) 153–162.

665 [92] J.J. Calvin, M. Asplund, Y. Zhang, B. Huang, B.F. Woodfield, Heat capacity and thermodynamic  
666 functions of  $\gamma$ -Al<sub>2</sub>O<sub>3</sub>, *J Chem Thermodyn.* 112 (2017) 77–85.

667 [93] S. Ghazizadeh, T. Hanein, J.L. Provis, T. Matschei, Estimation of standard molar entropy of  
668 cement hydrates and clinker minerals, *Cem Concr Res.* 136 (2020) 106188.

669